Subband gap impact ionization and excitation in carbon nanotube transistors

Jing Guo[a)]
Department of Electrical and Computer Engineering, University of Florida, Gainesville, Florida 32611

Muhammad A. Alam
School of Electrical and Computer Engineering, Purdue University, West Lafayette, Indiana 47907

Yijian Ouyang
Department of Electrical and Computer Engineering, University of Florida, Gainesville, Florida 32611

(Received 6 September 2006; accepted 12 December 2006; published online 23 March 2007)

Impact excitation (IE) and impact ionization (II) play important roles in carbon nanotube (CNT) optoelectronics and device reliability. The Boltzmann transport equation (BTE) in both the real and k spaces is solved to study subband gap II and IE in a CNT metal-oxide-semiconductor field-effect transistor (MOSFET). We show that even when the band bending is smaller than the CNT band gap, considerable II or IE can occur. The subband gap II rate varies exponentially with the applied drain voltage, but the current varies linearly due to a small amount of excess carriers. In contrast, solving the BTE by assuming a constant electric field indicates that both the II rate and current varies exponentially. Subband gap II or IE explains why considerable light emission was observed even when the potential drop is smaller in a recent experiment on bright CNT light emitters. The observed exponential variation of light intensity versus the linear variation of current alone, however, is not sufficient to distinguish between subband gap II and subband gap IE. The results also indicate that the bias condition for the maximum hot carrier degradation in CNT MOSFETs is the same as in Si MOSFETs. © *2007 American Institute of Physics*. [DOI: 10.1063/1.2435821]

I. INTRODUCTION

Single walled carbon nanotubes (CNTs) have been extensively explored for device applications due to their excellent electrical, optical, and mechanical properties.[1] The progress on CNT optoelectronic devices has been rapid,[2–6] since the first demonstration of a CNT infrared emitter.[7] Theoretical models and simulators have been developed to understand the operation of CNT optoelectronic devices.[8] It has been recently shown that significant improvement of quantum efficiency can be achieved for a CNT light emitter by using a suspended CNT channel operating in the unipolar transport regime.[4] Since this remarkable quantum efficiency must arise from generation (and subsequent recombination) of electron-hole pairs created by energetic unipolar source-drain current, a careful consideration of both impact excitation (IE) (leading to bounded electron-hole pairs) and impact ionization (II) (leading to free electron-hole pairs) is obviously necessary. In addition, impact ionization also plays an important role on device reliability.

A simple model, which computes the impact excitation rate as $\sim\exp(-\varepsilon_{\rm th}/\varepsilon)$ (where $\varepsilon_{\rm th}$ is the threshold electric field and ε is the electric field), has been used to compute the impact excitation rate at the edge of the suspended CNT trench.[4] Since the expression is strictly valid for bulk semiconductors with spatially uniform electric fields, its validity for the suspended CNT device[4] needs to be carefully examined for the following two reasons: First, since the electric field varies rapidly with position at the edge of the trench (the electrostatic screening length was estimated to be $\sim$20 nm),[4] analysis of the IE in terms of a constant electric field may not be appropriate. Second, the band bending at the edge of the trench, which was estimated to be about the band gap energy, E_g, is smaller than the IE threshold energy. The IE formula, $\sim\exp(-\varepsilon_{\rm th}/\varepsilon)$, therefore, would not hold under these conditions.

A microscopic description of carrier transport is needed to address the earlier concerns. A Boltzmann transport equation (BTE) in k space only (i.e., bulk semiconductor) has been previously solved to model IE in the device,[4] but the real-space dependence must be explicitly included because the electric field varies rapidly with the position. In this work, we directly solve the BTE in both the real and k spaces for a CNT metal-oxide-semiconductor (MOS) field-effect transistor (FET). We show that even when the potential drop is smaller than the CNT band gap, considerable subband gap II (or IE) can occur near the channel-drain junction. The subband gap II (or IE) rate varies exponentially with the applied drain voltage, but since the magnitude of the excess carriers is small, the source-drain current still varies linearly with the applied drain voltage. The result is in agreement with previous studies on subband gap II in Si MOSFETs,[9,10] and provides another mechanism (besides the exciton picture) that can also be responsible for the linear variation of the current versus the exponential variation of the light intensity in the CNT light emitter experiment.[4] Although subband gap IE is certainly possible as well, we show that the basic features of the current-voltage characteristics and emission intensity can be adequately described by subband gap II alone. We also show that the subband gap II (or IE) rate

a)Electronic mail: guoj@ufl.edu

 © 2007 American Institute of Physics

Downloaded 11 Jan 2008 to 128.46.94.119. Redistribution subject to AIP license or copyright; see http://jap.aip.org/jap/copyright.jsp

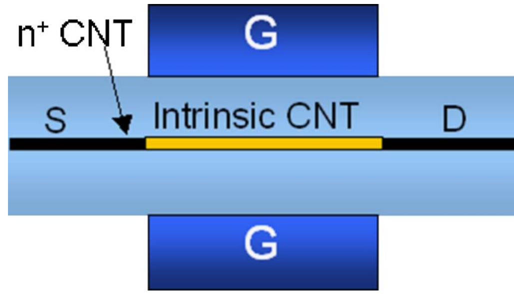

FIG. 1. (Color online) The modeled CNTFET: The (22, 0) CNT has a diameter of ~1.72 nm, which results in a band gap of ~0.48 eV. The channel length is 20 nm. The simulated source/drain extension has a length of $L_{sd}=30$ nm and a donor doping density of $N_D=5\times10^8$/m. The high-κ gate insulator thickness is 5 nm and the dielectric constant is 16.

reaches a maximum value when the gate voltage is about one half of the drain voltage due to two competing mechanisms.

II. APPROACH

The modeled device is a coaxially gated CNT MOSFET as shown in Fig. 1. The (22, 0) zigzag intrinsic CNT channel has a diameter of 1.72 nm, which results in a band gap of about 0.48 eV. The intrinsic channel length is $L_{ch}=20$ nm and the simulated source and drain extensions have a length of $L_{sd}=30$ nm and a donor doping density of $N_D=5\times10^8$/m. The high-κ gate insulator thickness is 5 nm and the dielectric constant is 16. The flatband voltage is zero.

The BTE was solved for the whole CNT using the finite difference method at the steady state

$$-\frac{q\varepsilon(x)}{\hbar}\frac{\partial f(x,k)}{\partial k}+\upsilon(k)\frac{\partial f(x,k)}{\partial x}=\hat{c}f(x,k), \tag{1}$$

where $f(x,k)$ is the carrier distribution function, x is the position, k is the wave vector, $\varepsilon(x)$ is the electric field, $\upsilon(k)$ is the carrier velocity, q is the electron charge, and $\hat{c}f(x,k)$ is the collision integral operating on the distribution function. The BTE has been previously applied to study 10 nm scale Si MOSFET and validated by detailed quantum transport simulations.

Descriptions of the CNT band structrue and scattering rate are needed to solve the BTE. The band structure of the ith conduction subband is described by the following expression derived from the p_z tight binding approximation:[11]

$$E_i(k)=\hbar\upsilon_F(\sqrt{k^2+k_i^2}-k_i), \tag{2}$$

where $E_i(k)$ is the carrier kinetic energy, $\hbar$ is the reduced Planck constant, $\upsilon_F\approx9.6\times10^7$ cm/s is the Fermi velocity, and $k_i=\{[6\times i-3-(-1)^i]\}\times[2/(3d)]$ is the quantized wave vector for the ith subband in the circumferential direction of the tube,[12] where d is the CNT diameter.

Phonon scattering and impact ionization are treated in the collision integral at the right-hand side of Eq. (1). Acoustic phonon (AP) scattering, which is nearly elastic and has a long mean free path (mfp) of ~1 μm, is important under low bias conditions. We model the AP scattering as an elastic scattering process, which results in a collision integral term as

$$\hat{c}_{AP}f(k)=\frac{1}{\tau_{AP}(k_{i,AP})}f(k_{i,AP})[1-f(k)] - \frac{1}{\tau_{AP}(k)}f(k)[1-(k_{f,AP})], \tag{3}$$

where the first term describes in-scattering and $k_{i,AP}$ is the wave vector of initial state that results in a final state of k through AP scattering, the second term describes out-scattering and $k_{f,AP}$ is the final state wave vector, and $1/\tau_{AP}(k)$ is the AP scattering rate related to the AP scattering mfp.[13] The optical phonons (OPs) and the zone boundary (ZB) phonons have phonon energies between 160 and 200 meV, and result in OP/ZB scattering at high bias conditions.[13] We combine the OP scattering and the ZB scattering as an inelastic scattering process with an average phonon energy of $\hbar\omega_{OP/ZB}=180$ meV,

$$\hat{c}_{OP/ZB}f(k)=\frac{1}{\tau_{OP/ZB}(k_{i,OP/ZB})}f(k_{i,OP/ZB})[1-f(k)] - \frac{1}{\tau_{OP/ZB}(k)}f(k)[1-f(k_{f,OP/ZB})], \tag{4}$$

where $k_{i,OP/ZB}$ ($k_{f,OP/ZB}$) is the initial (final) state wave vector, which results in (from) a scattering final (initial) state of k, and $1/\tau_{OP/ZB}$ is the total OP and ZB scattering rate. Only OP emission is treated because self-heating is not important for a nonsuspended CNT under modest biases.

Impact ionization (or impact excitation)[14] is treated similarly as a scattering mechanism with an empirical rate of[15]

$$\frac{1}{\tau_{II}(E)}=\frac{P}{\tau(E_{th})}\left(\frac{E-E_{th}}{E_{th}}\right)^{\beta}, \tag{5}$$

where E_{th} is the threshold energy for II (or IE), and $1/\tau(E_{th})$ is the scattering rate at $E=E_{th}$, and P is a unitless factor much larger than 1. The difference between II and IE terms in the BTE is that they have different E_{th}, β, and P values. The dependence of the simulation results on E_{th} will be discussed later. Previous works indicate $\beta\approx2$ for II,[15] and we assume the same value for IE. Variation of β, does not change the qualitative features of the simulation results. When the factor P is large enough, the total II (or IE) rate is independent of its exact value.[15] A value of $P=50$ to ∞ has been used for conventional semiconductors.[15] Here we use $P=1000$. The earlier model provides a phenomenological description of the rates near E_{th} and a rigorous calculation of the II and IE rates has been reported recently.[14]

The following boundary condition is imposed to the BTE. The carrier distribution function at the left end of the source extension is determined by the source Fermi–Dirac distribution function. Similarly, the distribution function at the right end of the drain extension is determined by the drain Fermi–Dirac distribution function. In order to treat self-consistent electrostatics, the BTE is iteratively solved with a two-dimensional Poisson equation in the cylindrical coordinates until convergence is achieved for each bias point. The source-drain current, and II (or IE) rate are then computed.

Downloaded 11 Jan 2008 to 128.46.94.119. Redistribution subject to AIP license or copyright; see http://jap.aip.org/jap/copyright.jsp

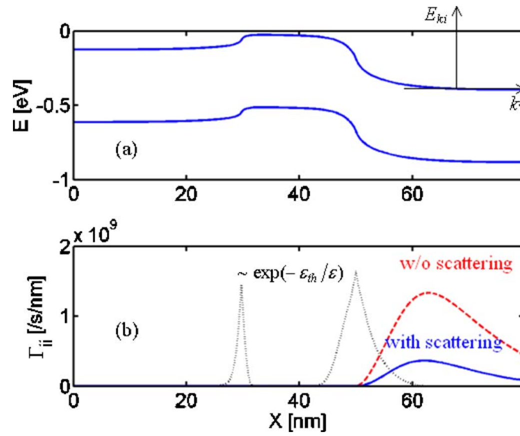

FIG. 2. (Color online) Subband gap impact ionization vs position: (a) The conduction and valence band profiles and (b) the impact ionization rate per unit channel length vs the position at $V_D = V_G = 0.3$ V. The left end of the simulated source extension is defined as $x = 0$. The dashed line is without phonon scattering and the solid line is with phonon scattering. We also plotted the II rate computed by $\sim\exp[-\varepsilon_{th}/\varepsilon(x)]$ for comparison (the dotted line).

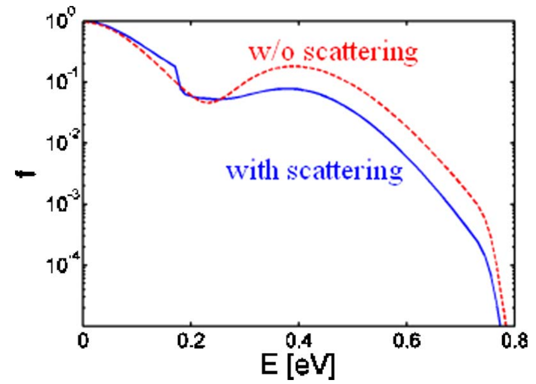

FIG. 3. (Color online) Effect of phonon scattering: The carrier distribution function vs the kinetic energy for the $+k$ states at $x = 70$ nm [see Fig. 2(a)].

III. RESULTS

We first examine the II rate as a function of the channel position. An II threshold energy of $E_{th} = 1.5E_g$ is used due to the requirement of energy and momentum conservations. (The effect of varying the threshold energy will be discussed in detail later.) Figure 2(a) plots the first conduction and valence subband profiles at $V_D = V_G = 0.3$ V. Because the conduction band bending at the channel-drain junction is smaller than the CNT band gap, one might expect that no II should occur. The dashed line in Fig. 2(b), which plots the simulated II rate versus the position without phonon scattering, however, indicates that a considerable amount of II occurs near the channel-drain junction and also inside the drain extension due to the high energy tail of the distribution functions. The II rate reaches a maximum value at $x = 60$ nm, which is inside the drain extension but close to the channel-drain junction. The width of the II peak, which is a few tens of nanometers in this simulation, is determined by the potential profile and the factor P in Eq. (5) (though the total II rate is insensitive to P when it is large enough). Subband gap II has been previously studied for nanoscale Si MOSFETs. It plays an important role in determining substrate current characteristics and device reliability, especially when Si MOSFETs scale down to the nanometer regime.[9]

In order to understand the mechanism of subband gap impact ionization, we plot the electron distribution function versus kinetic energy for the $+k$ states at $x = 70$ nm (20 nm away from the channel-drain junction), as shown by the dashed line in Fig. 3(a). The following three features can be identified. (1) For $E < 0.2$ V, the distribution function decreases due to the drain-injected, quasithermalized electrons. (2) A local maximum value appears around $E < 0.4$ V due to the source-injected, quasiballistic electron stream. (3) The slope of the exponentially decaying tail increases at $E_{th} \approx 0.73$ eV due to the onset of II. Although the potential drop at the channel-drain junction is smaller than the threshold energy for II, electrons in the high energy tail have enough energy to result in II.

We next explore the effect of phonon scattering on the subband gap II rate. The solid line in Fig. 2(b) compares the II rate versus the position in the presence of (the solid line) and without phonon scattering (the dashed line). After phonon scattering is included, the II rate decreases by a factor of ~ 4, with a similar curve shape. In order to understand the decrease of the II rate, we also plotted the carrier distribution function for the $+k$ states at $x = 70$ nm in the presence of phonon scattering as the solid line in Fig. 3. Compared to that without scattering, the distribution function decreases rapidly near the energy of $E \approx \hbar\omega_{OP/ZB}$ due to the onset of OP/ZB scattering. The fraction of electrons in the high energy tail is reduced. The II rate, therefore, decreases. For comparison, we also plotted the II rate computed by the simple equation $\sim\exp[-\varepsilon_{th}/\varepsilon(x)]$ as the dotted line in Fig. 2(b). It predicts a significantly different position-resolved II rate from that computed by a full solution to the BTE. A full solution of BTE, therefore, is necesarry to predict the II rate near the junction.

We next examine the dependence of subband gap II rate on the drain bias. Figure 4(b), which plots the impact ionization rate as a function of the drain voltage at $V_G = 0.3$ V, shows that the rate exponentially varies with the applied drain voltage. On the other hand, Fig. 4(c) shows that the source-drain current still varies linearly with the applied drain voltage. To understand the reason, Fig. 4(a) plots the conduction band profile versus the position at $V_G = 0.3$ V for different drain voltages. Because the subband gap II is due to the exponentially decaying high energy tail, the increase of potential drop at the channel-drain junction results in an *exponential* increase of the total II rate. On the other hand, the fraction of carriers in the high energy tail is small. The source-drain current is determined by most low-energy carriers that do not experience II, and therefore, varies linearly with the applied drain voltage. The exponential variation of the II rate versus the linear variation of the source drain current has been previously identified as a signature of subband gap II in nanoscale Si MOSFETs.[9,10] (In contrast, the earlier band gap II results in exponential variation for both the current and the total II rate.) Subband gap II (or IE) can also play an important role in the recent experiment on bright CNT light emitters, in which electron-hole pairs are generated by II (or IE) and subsequently recombine to emit light.

Downloaded 11 Jan 2008 to 128.46.94.119. Redistribution subject to AIP license or copyright; see http://jap.aip.org/jap/copyright.jsp

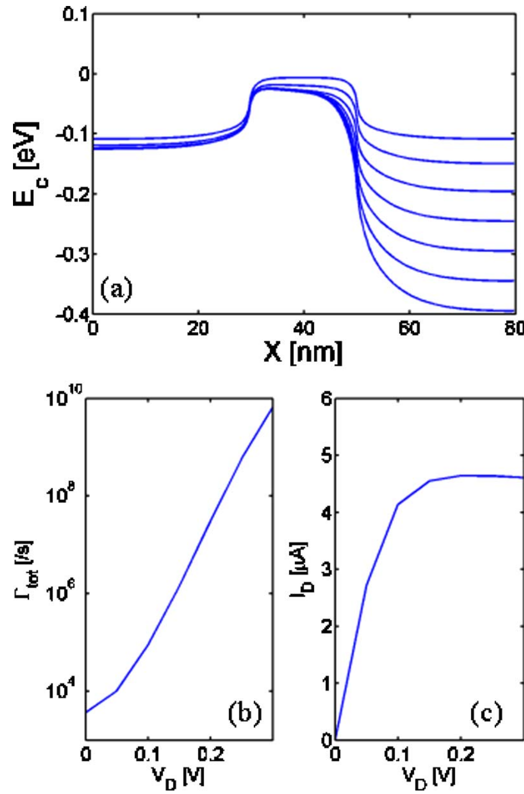

FIG. 4. (Color online) The drain voltage dependence: (a) The conduction band profile at V_G=0.3 V and V_D=0–0.3 V at 0.05 V/step. (b) The total impact ionization rate and (c) the source-drain current vs the applied drain bias V_D at V_G=0.3 V.

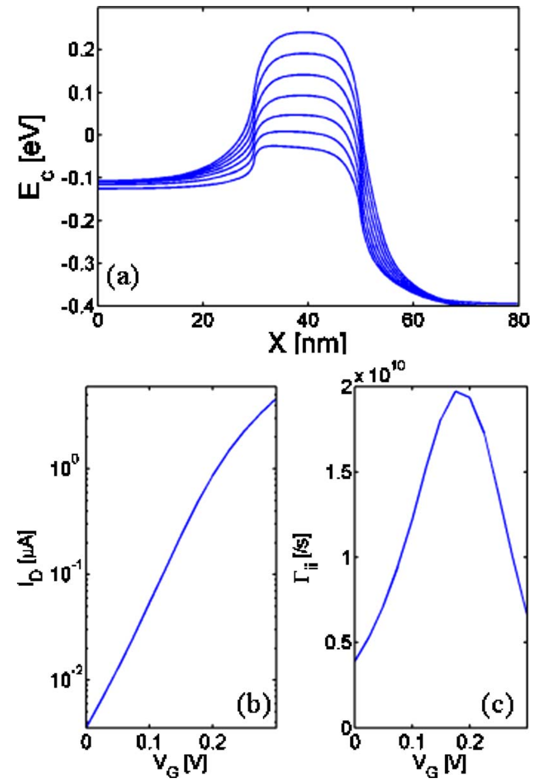

FIG. 5. (Color online) The gate voltage dependence: (a) The conduction band profile at V_D=0.3 V and V_G=0–0.3 V at 0.05 V/step. (b) The source-drain current and (c) the total impact ionization rate in the CNT vs the applied gate bias V_G at V_D=0.3 V.

The potential drop is estimated to be close to the band gap, which is smaller than the II (or IE) threshold energy. The light intensity (which is proportional to the total II or IE rate) exponentially varies when the source-drain current linearly varies, which can be partly due to the reason as explained earlier.

We explore the dependence of the rate on the applied gate voltage next. Figure 5(c), which plots the total II rate versus the gate voltage, shows that a maximum impact ionization rate is reached when V_G is approximately $V_D/2$. To understand the reason, Fig. 5(a) plots the conduction band profile at V_D=0.3 V and different gate voltages, and Fig. 5(b) plots the source-drain current versus the gate voltage. As V_G increases, the current exponentially increases in the subthreshold region, but the rate first increases and then decreases due to the following two competing mechanisms. First, the increase of the source-drain current tends to increase the total II rate as V_G increases. Second, the band bending at the channel-drain junction decreases when V_G increases, as shown in Fig. 5(c), which results in a decrease of the II rate. For $V_G < V_D/2$, the first effect dominates and the rate increases with V_G. For $V_G > V_D/2$, the second effect dominates and the rate decreases with V_G. The maximum impact ionization is reached near $V_G = V_D/2$. Because II can be an important mechanism that leads to the reliability problem, the hot carrier degradation is most severe when a CNTFET is biased at $V_G \approx V_D/2$. The bias condition for severe hot carrier degradation is the same as that for Si MOSFETs, which has been experimentally verified.[16]

We finally examine the dependence of II (or IE) rate on threshold energy E_{th}, as shown in Fig. 6. For II, $E_{th} = \alpha E_g$, where the unitless factor $\alpha \approx 1.5$ is due to the requirement of simultaneous energy and momentum conservations. The exact value of α varies for different materials and different types of carriers, but it must be larger than 1 due to the requirement of energy conservation. For IE in a CNT, $E_{th} = 1.6 E_g$ was reported due to the requirement of energy and angular momentum conservation.[4] Interaction with the gate oxide and exciton band mixing effect may relax the requirement to $E_{th} \approx E_g$. We define the II (or IE) efficiency as η

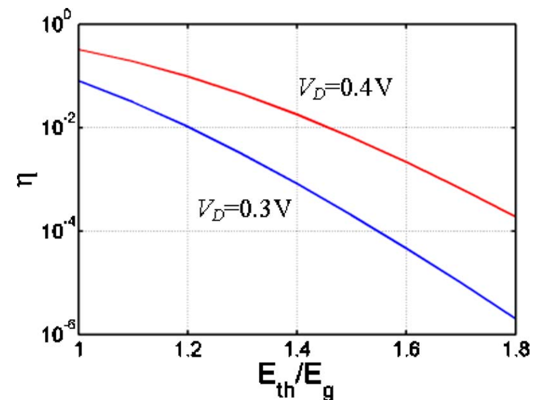

FIG. 6. (Color online) Effect of the threshold energy: The II (or IE) efficiency as a function of the normalized threshold energy E_{th}/E_g at V_G =0.3 V and V_D=0.3 V and 0.4 V, where $E_g \approx 0.48$ eV is the first subband gap. The potential drop at the channel-drain junction is about 0.37 eV at V_D=0.3 V and 0.46 eV at V_D=0.4 V.

Downloaded 11 Jan 2008 to 128.46.94.119. Redistribution subject to AIP license or copyright; see http://jap.aip.org/jap/copyright.jsp

$=q\Gamma_{\rm tot}/I_D$, where $\Gamma_{\rm tot}$ is the total II (or IE) rate in the channel and I_D is the source-drain current. When the potential drop at the channel-drain junction is smaller than the band gap, the efficiency is much smaller than 1 and exponentially decreases as $E_{\rm th}$ increases. The efficiency at $V_D=0.4$ V (which results in a potential drop of 0.45 eV at channel-drain junction), however, is still about 6.47×10^{-3} at $E_{\rm th}=1.5E_g$ (as shown in Fig. 6), which is on the same order of magnitude as the experimentally characterized light emission efficiency for a suspended CNT channel with similar tube diameter and potential drop.[4] The efficiency can be significantly improved if $E_{\rm th}$ can be engineered to a lower value, or the potential drop over the junction can be increased.

IV. CONCLUSIONS AND DISCUSSIONS

We show that considerable subband gap II or IE can occur even when the potential drop is smaller than the band gap for a CNT device. In the presence of subband gap II, the source-drain current still varies linearly with the applied drain bias, but the total II rate exponentially varies. The qualitative feature cannot be obtained by solving BTE in k space only by assuming a constant electric field. Because the potential drop in a recent experiment on light emission from suspended CNTs is small, subband gap IE or subband gap II are likely to be responsible for electron-hole pair generation. The exponential variation of light intensity versus the linear variation of current alone, however, is not sufficient to distinguish between subband gap IE and subband gap II. Stronger electrostatic screening (due to a larger carrier density induced by the gate), larger electric field, self-heating effects,[6] and incoherent scatterings can make excitons less stable in electroluminescence (EL) devices than in photoluminescence (PL) experiments.[17,18] This work shows that subbandgap impact ionization alone can provide a plausible explanation for the linear variation of the current versus the exponential variation of light emission intensity.

ACKNOWLEDGMENTS

The authors would like to thank D. Mann and Professor H. Dai of Stanford University and S. Koswatta of Purdue University for technical discussions.

[1] P. Avouris, J. Appenzeller, R. Martel, and P. Avouris, Proc. IEEE **91**, 1772 (2003); P. L. McEuen, M. S. Fuhrer, and H. K. Park, IEEE Trans. Nanotechnol. **1**, 78 (2002).
[2] M. Freitag, J. Chen, J. Tersoff, J. Tsang, Q. Fu, J. Liu, and Ph. Avouris, Phys. Rev. Lett. **93**, 076803 (2004).
[3] J. U. Lee, Appl. Phys. Lett. **87**, 073101 (2005); M. Freitag, V. Perebeinos, J. Chen, A. Stein, J. Tsang, J. Misewich, R. Martel, and Ph. Avouris, Nano Lett. **4**, 1063 (2004).
[4] J. Chen, V. Perebeinos, M. Freitag, A. Carlsen, J. Chen, A. Troeman, H. Hilgenkamp, and Ph. Avouris, Science **310**, 1171 (2005).
[5] M. Freitag, J. C. Tsang, J. Kirtley, J. Tsang, Q. Fu, J. Liu, and Ph. Avouris, Nano Lett. **6**, 1425 (2006).
[6] D. Mann *et al.*, Nature Nanotechnology **2**, 33 (2007).
[7] J. A. Misewich, R. Martel, P. Avouris, J. Tsang, S. Heinze, and J. Tersoff, Science **300**, 783 (2003).
[8] J. Guo and M. A. Alam, Appl. Phys. Lett. **86**, 023105 (2005); J. Tersoff, M. Freitag, J. C. Tsang, and Ph. Avouris, Appl. Phys. Lett. **86**, 263108 (2005); D. McGuire and D. L. Pulfrey, Nanotechnology **17**, 5805 (2006); C. T. Hsieh, D. S. Citrin, and P. P. Ruden, Appl. Phys. Lett. **90**, 012118 (2007).
[9] K. G. Anil, S. Mahapatra, and I. Eisele, Solid-State Electron. **47**, 995 (2003).
[10] M. V. Fischetti, S. E. Laux, and E. Crabbe, J. Appl. Phys. **78**, 1058 (1995).
[11] J. W. Mintmire and C. T. White, Phys. Rev. Lett. **81**, 2506 (1998).
[12] J. Guo, S. Goasguen, M. Lundstrom, and S. Datta, Appl. Phys. Lett. **81**, 1486 (2002).
[13] A. Javey, J. Guo, M. Paulsson, W. Qian, D. Mann, M. Lundstrom, and H. Dai, Phys. Rev. Lett. **92**, 106804 (2004); J. Y. Park, S. Rosenblatt, Y. Yaish, V. Sazonova, H. Ustunel, S. Braig, T. Arias, P. Brouwer, and P. L. McEuen, Nano Lett. **4**, 517 (2004).
[14] V. Perebeinos and P. Avouris, Phys. Rev. B **74**, 121410 (2006).
[15] J. Y. Tang and K. Hess, J. Appl. Phys. **54**, 5139 (1983).
[16] C. M. Hu, S. C. Tam, F. C. Hsu, P. Ko, T. Chan, and K. W. Terrill, IEEE Trans. Electron Devices **32**, 375 (1985).
[17] F. Wang, G. Dukovic, L. E. Brus, and T. Heinz, Science **308**, 838 (2005).
[18] S. M. Bachilo, M. S. Strano, C. Kittrell, R. Hauge, R. Smalley, and R. Weisman, Science **298**, 2361 (2002).

Downloaded 11 Jan 2008 to 128.46.94.119. Redistribution subject to AIP license or copyright; see http://jap.aip.org/jap/copyright.jsp